

ADVANCED ENERGY MATERIALS

Supporting Information

for *Adv. Energy Mater.*, DOI: 10.1002/aenm.201903653

Light Absorption and Recycling in Hybrid Metal Halide Perovskite Photovoltaic Devices

*Jay B. Patel, Adam D. Wright, Kilian B. Lohmann, Kun Peng, Chelsea Q. Xia, James M. Ball, Nakita K. Noel, Timothy W. Crothers, Jenny Wong-Leung, Henry J. Snaith, Laura M. Herz, and Michael B. Johnston**

Supporting Information

**Light Absorption and Recycling in Hybrid Metal-Halide Perovskites
Photovoltaic Devices**

*Jay B. Patel, Adam D. Wright, Kilian B. Lohmann, Kun Peng, Chelsea Q. Xia, James M. Ball, Nakita K. Noel, Timothy W. Crothers, Jenny Wong-Leung, Henry J. Snaith, Laura M. Herz and Michael B. Johnston**

Experimental details	Page 2
Figure S1- Scanning electron microscopy images	Page 6
Figure S2- Determination of C_{60} thickness	Page 8
Figure S3- Urbach Energy	Page 9
Figure S4- Visible absorption spectra	Page 9
Figure S5- JV curves for champion devices	Page 10
Figure S6- Device statistics of all the devices	Page 11
Figure S7- Evaporation rate calculation	Page 11
Figure S8- Transient photoluminescence & THz conductivity	Page 12
Figure S9- Series resistance and shunt resistance	Page 12
Figure S10- SnO_2 device current-voltage curve	Page 13
Figure S11- Migration of Ag in devices	Page 13
Figure S12- Internal quantum efficiency	Page 14
Figure S13- Optical Simulations	Page 15
Figure S14- Comparison of Current Densities	Page 16

Experimental

Substrate Cleaning

Fluorine doped tin oxide (FTO, Tec 15 Hartford Glass) substrates, were washed using Hellmanex, acetone (Sigma Aldrich), isopropanol (Sigma Aldrich), and ethanol (Sigma Aldrich), in that order. The substrates were then placed in the oxygen plasma etcher for 10 minutes.

SnO₂

SnO₂ was prepared as reported previously.^[1] Briefly SnCl₄·5H₂O in IPA (0.05 M) was spin coated on the clean FTO substrates at 3000 RPM and then annealed at 180°C for 1 hour. The substrates were then placed in a chemical bath consisting of SnCl₂·2H₂O (108 mg), 3-Mercaptopropionic acid (10 µl) deionized water (40 ml), Urea (500 mg) and 37% HCl (500 µl). The chemical bath containing the substrates were placed in an oven for 3 hours at 70°C. Afterwards, the films were washed with deionized water and annealed for 1 hour at 180°C

C₆₀

C₆₀ was thermally evaporated as described previously.^[2] In brief, C₆₀ was placed in a crucible in a thermal evaporator. The C₆₀ was deposited at a rate of 0.05 Ås⁻¹ for 2000 s.

Perovskite Thin Films

The perovskite was deposited using thermal co-evaporation on the substrates as described below.

Spiro-OMeTAD

73 mg/ml of 2,2',7,7'-tetrakis-(N,N-di-p-methoxyphenylamine)9,9'-spirobifluorene (spiro-OMeTAD) was dissolved in chlorobenzene. Thereafter 38 µl lithium bis(trifluoromethanesulfonyl)imide (170 mg/mL in 1-butanol solution) was added along with 21 µl of 4-tert-butylpyridine (TBP) to 1 ml of Spiro-OMeTAD solution. The solution was then spincoated in a nitrogen filled glovebox at 2000 rpm for 45 seconds. The films were left to oxidized in a desiccator for 24 hours.

Electrodes

100 nm Silver contacts were thermally evaporated with a shadow mask for the devices. The base pressure was allowed to reach 10⁻⁶ mbar before initiating the evaporation. For the devices used to measure the absorption, external quantum efficiency and scanning electron microscopy, 100 nm gold electrodes were evaporated.

Perovskite thermal evaporation

CH₃NH₃I synthesis

20 ml methylamine (CH₃NH₂) solution 33 wt.% in absolute ethanol (Sigma Aldrich) was reacted with 31.8 ml of hydroiodic acid wt 57% in water. The methylamine solution was added dropwise into the hydroiodic solution. Thereafter the mixed solution was placed in a rotary evaporator for approximately 30 mins to evaporate the solvent and isolate the MAI salt. The methylammonium iodide (CH₃NH₃I) crystals were subsequently recrystallized in hot ethanol and then left in the fridge overnight and in the freezer for 5 hours thereafter. Large crystals were formed, which were washed with 200 ml diethyl ether and filtered in a Büchner flask, this was repeated for 3 times. The crystals of CH₃NH₃I were placed in a vacuum atmosphere overnight.

CH(NH₂)₂I and PbI₂

Formamidinium iodide was purchased from Dyesol and PbI₂ beads (99.999% metal bases) was purchased from Alpha Aesar.

Thermal co-evaporation

The organic precursor was placed in a ceramic crucible. Each deposition used fresh material, whereby the quantity used was based on the desired thickness of the perovskite. Approximately 300 nm of perovskite thin film required 300 mg of CH₃NH₃I. The PbI₂ was placed in another ceramic crucible. The samples were loaded in the evaporator on a temperature controlled, rotating substrate holder. The vacuum chamber was pumped down to $\sim 1 \times 10^{-6}$ mbar and the deposition rates for the PbI₂ was set at 0.4 \AA s^{-1} once the rate was stabilized the organic precursor deposition rate was set at 0.4 \AA s^{-1} and left to stabilize for ~ 40 mins. Thereafter the substrates were exposed to the vapor for a set amount of time (as shown in Figure S7) yielding different thicknesses of perovskite thin films.

Device Characterization

The solar cells were measured under simulated AM 1.5, 100 mW cm^{-2} sunlight (1 sun), using an ABET Technologies Sun 2000 and a Keithley 2400 Sourcemeter in ambient conditions. The active area of each device was defined by a mask which exposed a 0.0919 cm^2 active area for testing of both the current voltage characteristics and stabilized power output. The devices were prebiased at 1.4 V for 5 s before initiating the reverse and forward scans. Immediately after the J–V measurements, the SPO was measured without prebiasing. The devices were

kept at the voltage defined/ or close to (~ 0.7 V) the maximum power, which was determined from the J - V scans.

Fourier Transform Infrared/ Photocurrent Spectroscopy

Fourier transform infrared/ photocurrent spectroscopy (FTIR/FTPS) was carried out using a Bruker 80V interferometer. An Oriel class AAA solar simulator was used as the illumination source. For absorption measurements, a reflection and transmission unit were used, where a silver mirror was used as the reference for reflectance and vacuum was used as transmission. For the external quantum efficiency measurement (EQE), photocurrent of the perovskite thin film devices was measured using an aperture of 0.0625 cm^2 , and the spectra were corrected using a Newport calibrated silicon solar cell with a known EQE.

The *absorptance* spectra in Figure 2 for the devices were calculated as $A=1-R$. The *absorbance* spectra for the perovskite thin films (Figure S4) were calculated with $A_{10}=-\log(T/(1-R))$.

Photoluminescence Measurements

The samples were photoexcited in air by a 398 nm picosecond pulsed diode laser (PicoHarp, LDH-D-C-405M). The resultant PL was collected and coupled into a grating spectrometer (Princeton Instruments, SP-2558), which directed the spectrally dispersed PL onto an iCCD (PI-MAX4, Princeton Instruments) or a photon-counting detector (PDM series from MPD), whose timing was controlled with a PicoHarp300 TCSPC event timer. Laser fluences of 300 nJ cm^{-2} and 3 nJ cm^{-2} were used when obtaining the PL spectra and transient PL decay traces respectively.

Photon Reabsorption Calculations

The photon reabsorption-corrected spectra were obtained by using the ray-tracing model described by Crothers *et al.*^[3] The model calculates how much of the emitted PL is reabsorbed while travelling through the material, and how much is reflected or out-coupled at the interfaces. Light propagation is approximated to occur in only one dimension, and the model does not consider any light emitted as a result of reabsorption. The upper limit to the distance a ray can travel in the model is usually set to the scattering length scale, which is estimated from the inverse of the average below-bandgap absorption coefficient of the films: less than $30 \text{ }\mu\text{m}$ for the most strongly-scattering sample. To calculate the internally-emitted PL from the PL spectra measured a lateral distance of 1 mm away from the excitation spot, this maximum travel distance was set to 1 mm and out-coupling minimised in order to simulate a

lateral travel distance of 1 mm within the confines of the one-dimensional model. The model accounts for only one reabsorption event, however there may be multiple reabsorption events before out-coupling.

Optical-Pump-Terahertz-Probe Spectroscopy (OPTPS)

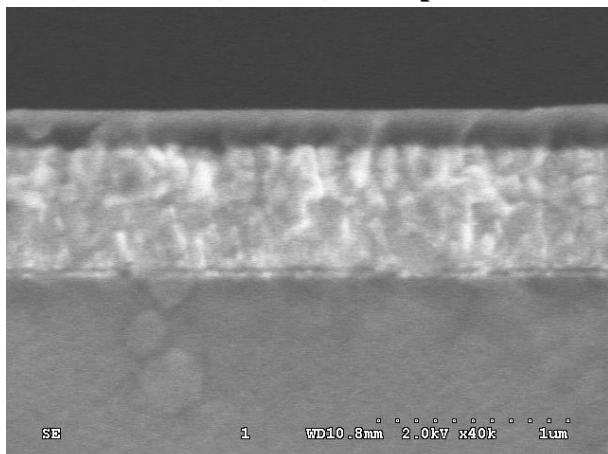
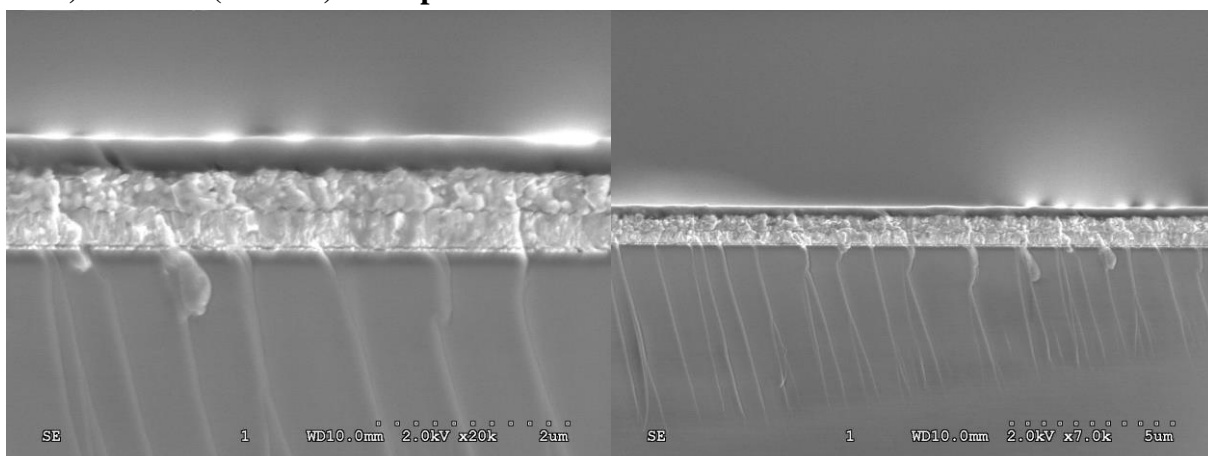
OPTPS was used to measure the charge-carrier mobilities of MAPbI₃ thin films with different thicknesses on z-cut quartz.^[4] An amplified laser with a central wavelength 800 nm, 35 fs pulse duration and 5 kHz repetition rate were split into three paths: THz beam, pump beam and gate beam. The THz pulse was generated by a spintronic emitter due to inverse spin hall effect^[5] and was detected using electro-optic sampling with a 1mm-thick ZnTe (110) crystal, a Wollaston prism and a pair of balanced photodiodes. The THz pulse was measured in reflection geometry. The pump beam was generated at 400 nm by a β -barium-borate (BBO) crystal to photoexcite the samples. The samples were photoexcited at various fluences ranging from 7.6 to 42.4 $\mu\text{J}/\text{cm}^2$

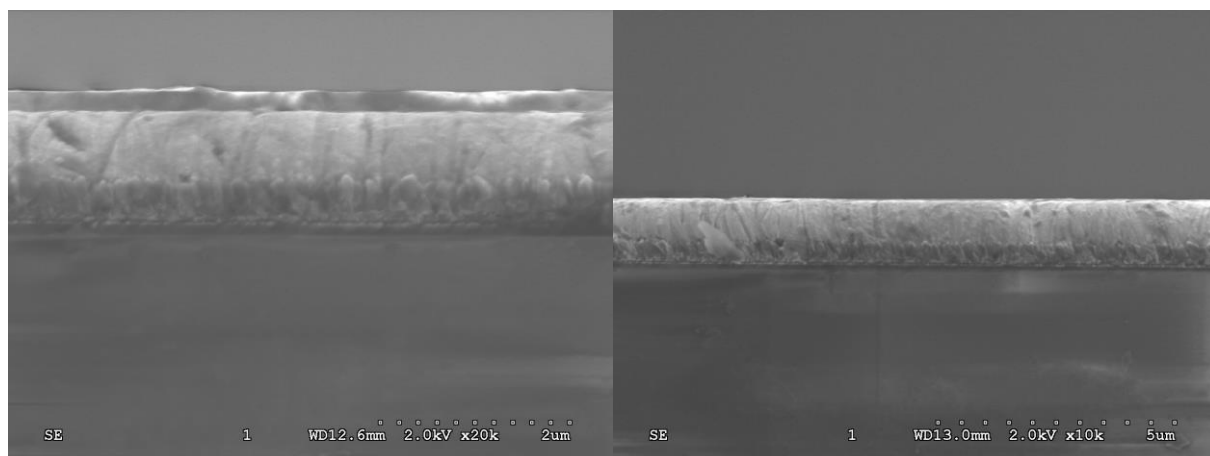
Scanning Electron Microscopy

Images were taken using a Hitachi S-4300 microscope using 2 kV accelerating voltage and 9 μA emission current. The detection method used was secondary electron detection. The thickness of the perovskite thin films in the devices were calculated by finding the mean thickness of 3 measurements across the cross-section SEM images in Figure S1.

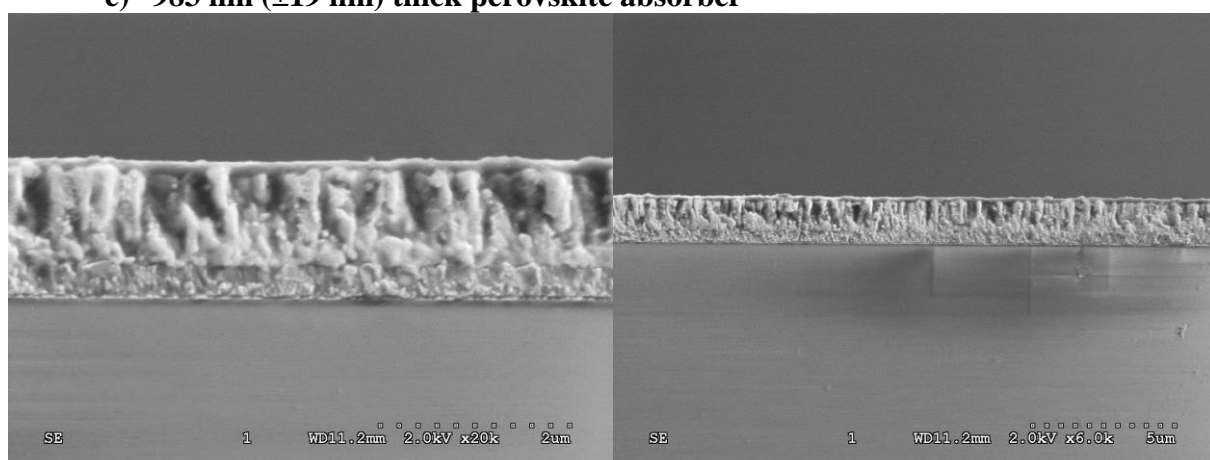
Scanning Transmission Electron Microscopy

Transmission electron microscopy samples were prepared by focused ion beam using a FEI Helios 600 Nanolab and the samples were analyzed using a JEOL 2100F instrument operated at 200 keV and equipped with scanning transmission electron microscopy (STEM) capabilities and the energy dispersive X-ray spectra (EDS) were collected using a JEOL silicon drift detector. The high angle annular dark field (HAADF) image of a cross-section of the solar cell shown in Fig. S11(a) was acquired using a 0.7nm spot size for the EDS maps shown in Figure S11(b-d).

Scanning Electron Microscopy Images**a) 67 nm (± 11 nm) thick perovskite absorber****b) 276 nm (± 25 nm) thick perovskite absorber****c) 412 nm (± 20 nm) thick perovskite absorber****d) 709 (± 24 nm) thick perovskite absorber**



e) 983 nm (± 19 nm) thick perovskite absorber



f) 1393 nm (± 13 nm) thick perovskite absorber

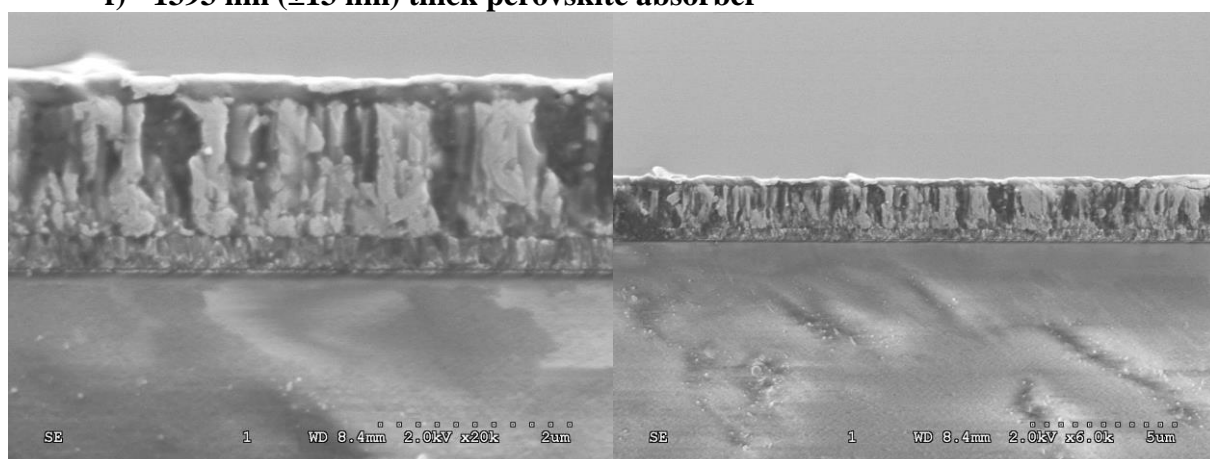


Figure S1. Scanning electron microscopy images of the cross section of the metal-halide perovskite devices used in this study. The images were used to calculate the thickness of the perovskite absorber layer

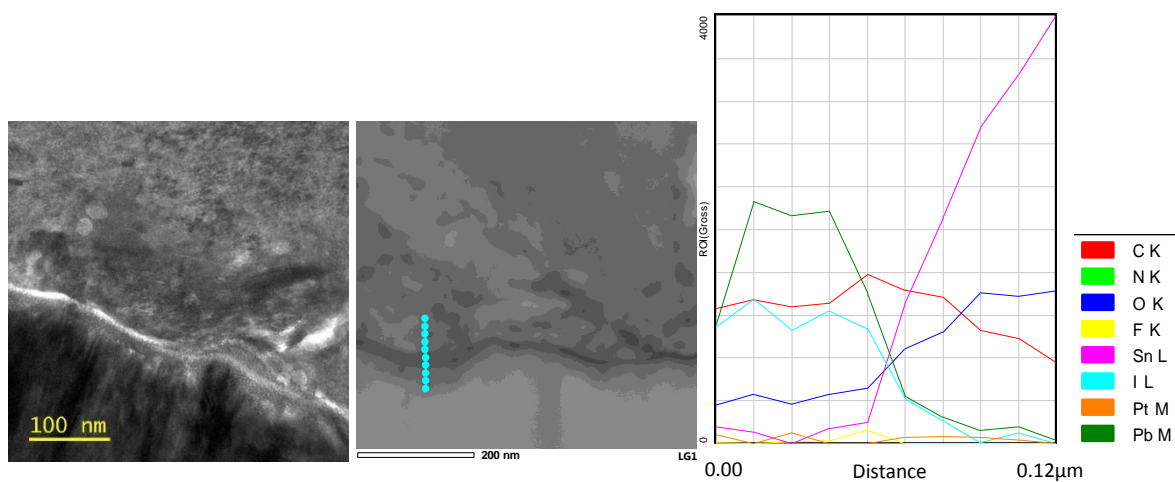


Figure S2. Line scan data, across the FTO/SnO₂/C₆₀ interface. The line scan shows and confirms the presence of C₆₀, as the C₆₀ layer is very thin (~10 nm). The colors in the line scan represent different chemical elements.

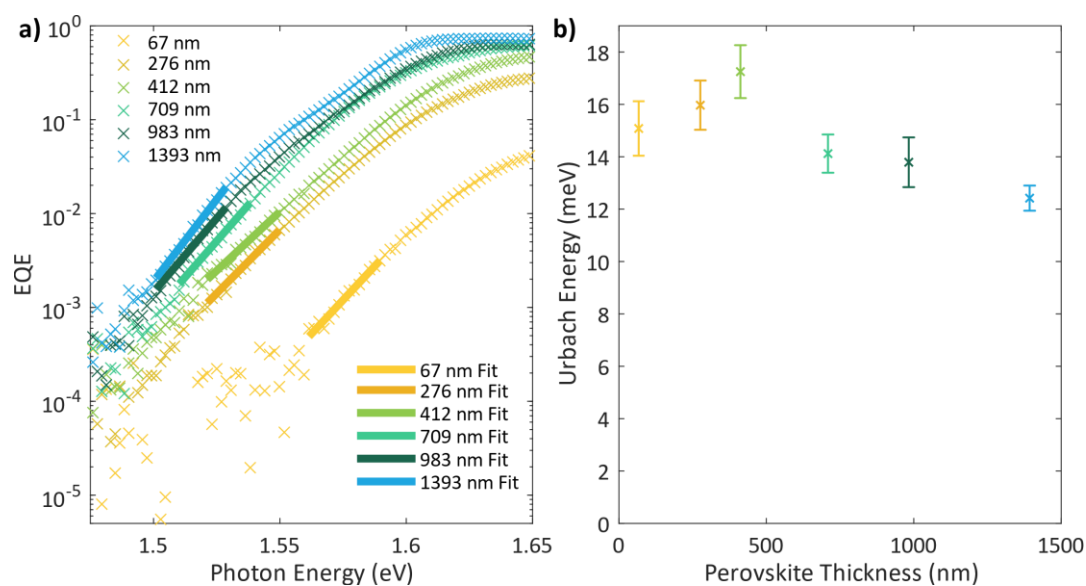


Figure S3 a) The Urbach fits of EQE spectra for devices shown in Figure 1 **b)** Dependence of the Urbach energy on absorber thickness for devices shown in Figure 1. The Urbach energy of the devices shows that there is significant reduction from 412 nm to 709 nm thick perovskite thin films. This corresponds with the observations in the SEM, where the morphology of the thin film changes to have large column-like structures. Moreover, as the perovskite films become thicker, there is an increase in EQE at lower photon energies due to less absorption losses as explained in the main text.

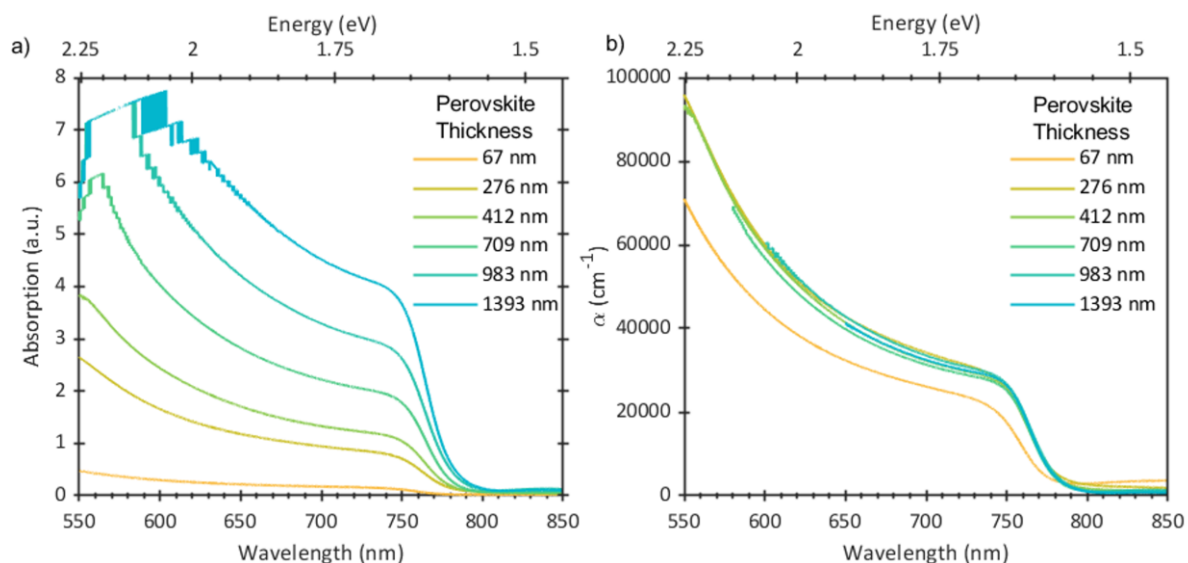


Figure S4. a) Absorption spectrum of the perovskite thin films on quartz **b)** the absorption coefficient (α) of the perovskite thin films. The difference in the absorption coefficient for the thinnest perovskite thin film (~ 67 nm) is can be attributed to the uncertainty in the value of thickness measured using SEM. The sharp step-like features at short wavelength arise from digitization.

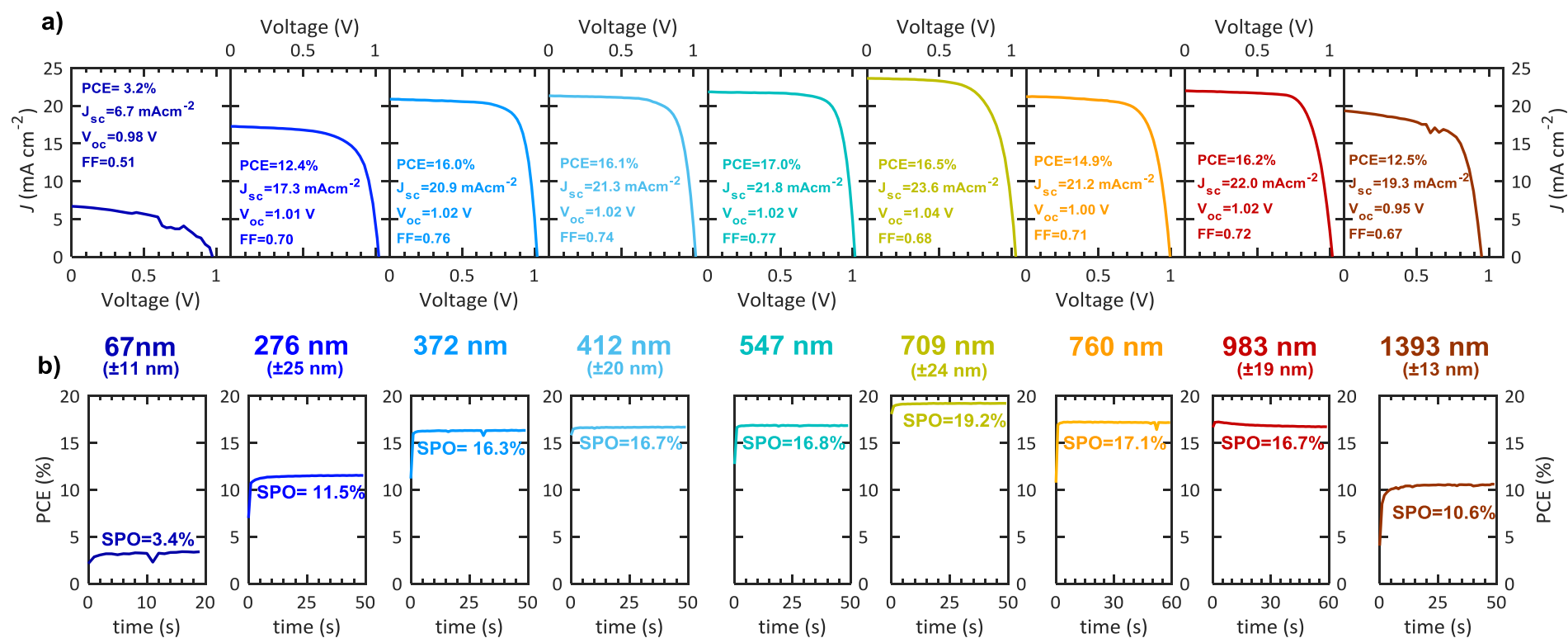


Figure S5. a) Current-Voltage curves of the champion devices of each thickness of perovskite absorber layer. The abbreviations stand for: power conversion efficiency (PCE), open circuit voltage (*V*_{oc}), short circuit current density (*J*_{sc}), fill factor (FF) b) the steady-state power output (SPO) of the champion devices. The devices showed an increase in PCE as they were light soaked, for ~10 s, as shown by the SPO data.

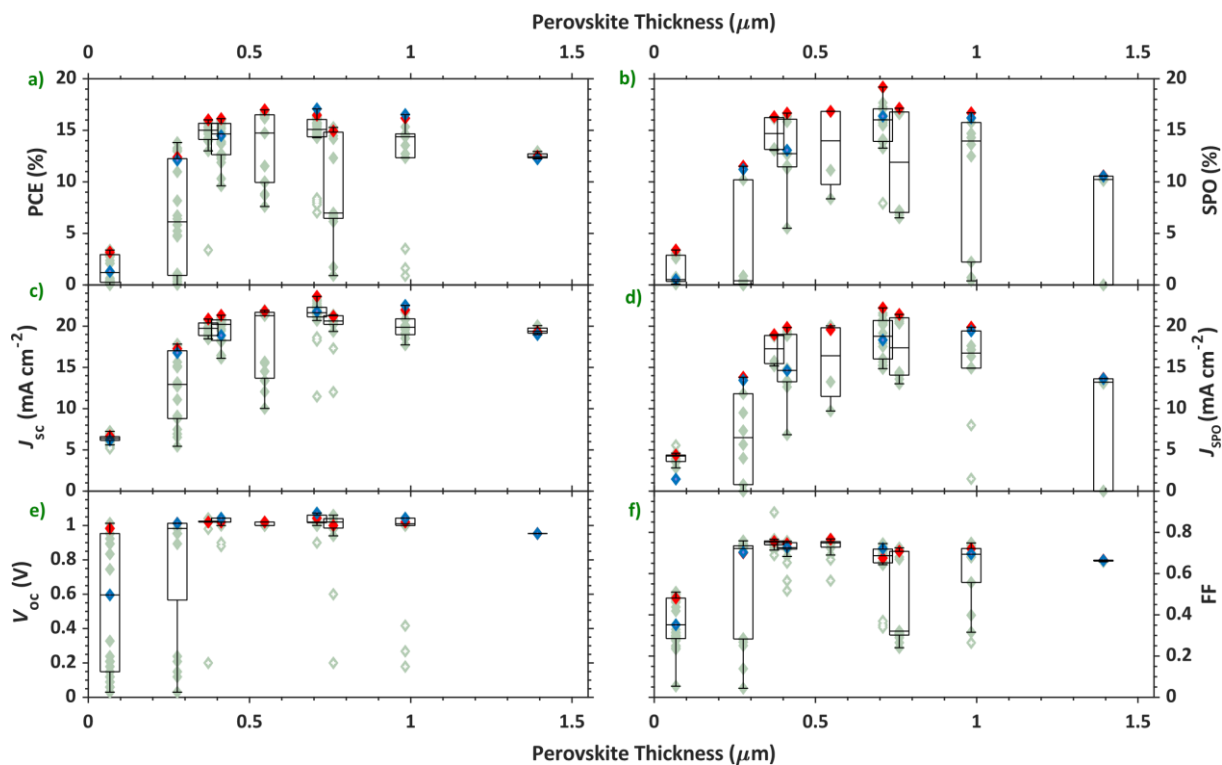


Figure S6. Performance parameters all the devices tested (green). **a)** Power conversion efficiency (PCE) **b)** Steady-state power output (SPO) **c)** Short circuit current density (J_{sc}) **d)** Steady-state current density (J_{spo}) **e)** Open circuit voltage (V_{oc}) **f)** Fill factor (FF). The data points in red are champion devices based on the highest stabilised power output and the blue data points show the device characteristics of the device absorption/EQE investigation (Figure 2). The boxplots were created using the standard MATLAB boxplot script.

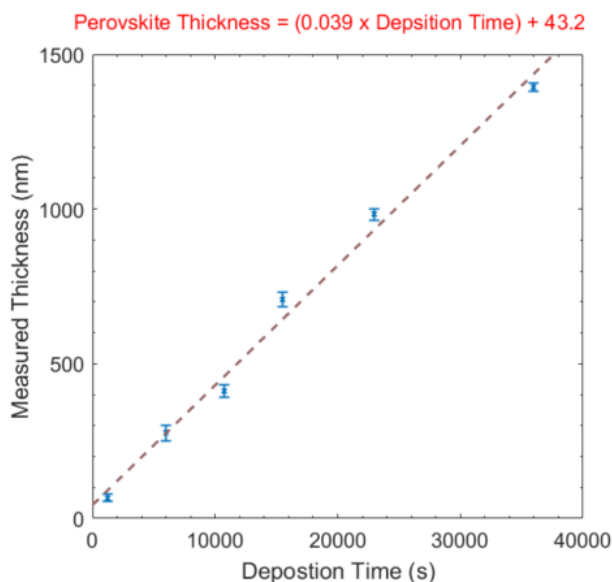


Figure S7. Shows the deposition rate calculated using the deposition time and the perovskite absorber thickness measured using SEM imaging. The linear fit was carried out using MATLAB.

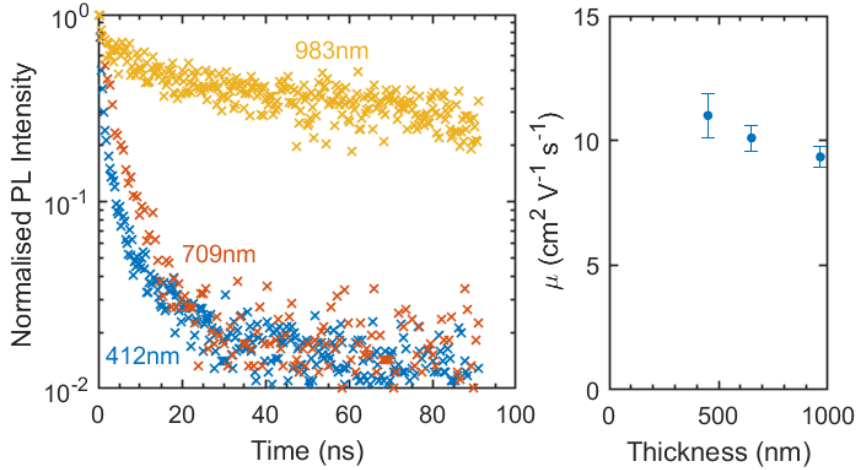


Figure S8. a) The transient photoluminescence decay traces for $\text{CH}_3\text{NH}_3\text{PbI}_3$ perovskite thin-films of different thickness on glass **b)** The charge-carrier mobility (μ), determined by THz conductivity measurements

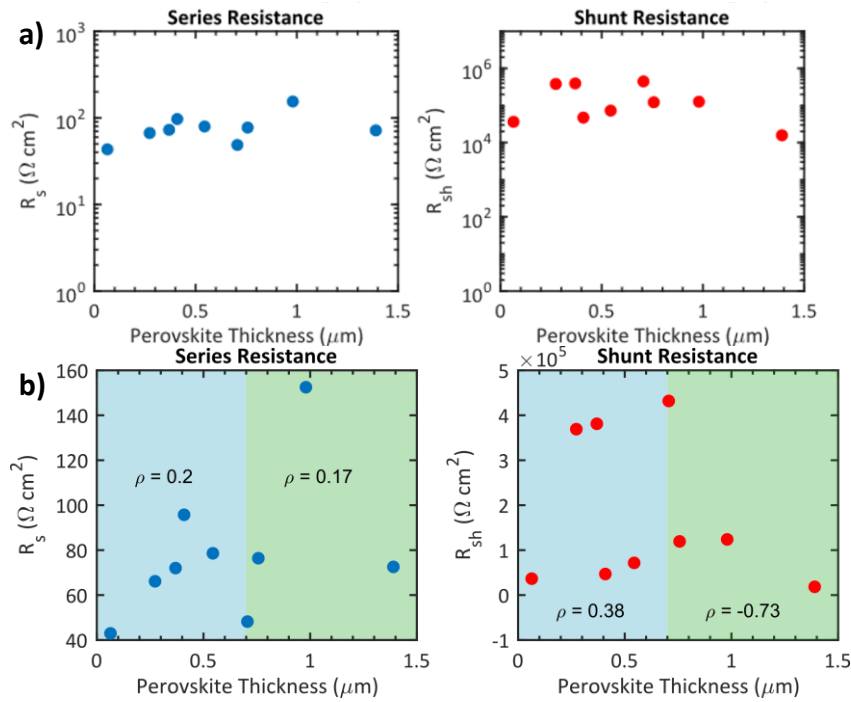


Figure S9 a) The series and shunt resistance (R_s and R_{sh} respectively) of the champion devices as shown in Figure S5. The resistance was estimated from the J - V curve by calculating the resistance. $R = \frac{1}{\left(\frac{dJ}{dV}\right)}$ where R_s is when $V=1.4$, and R_{sh} is when $V=0$ **b)** Correlation coefficients (ρ) between resistance and perovskite thin film thickness.

The series and shunt resistance were determined using the J - V curves show in figure S5. This method has been used before to understand the relative changes in the resistance of the devices,^[6,7] although impedance spectroscopy could also have been used.^[8,9]

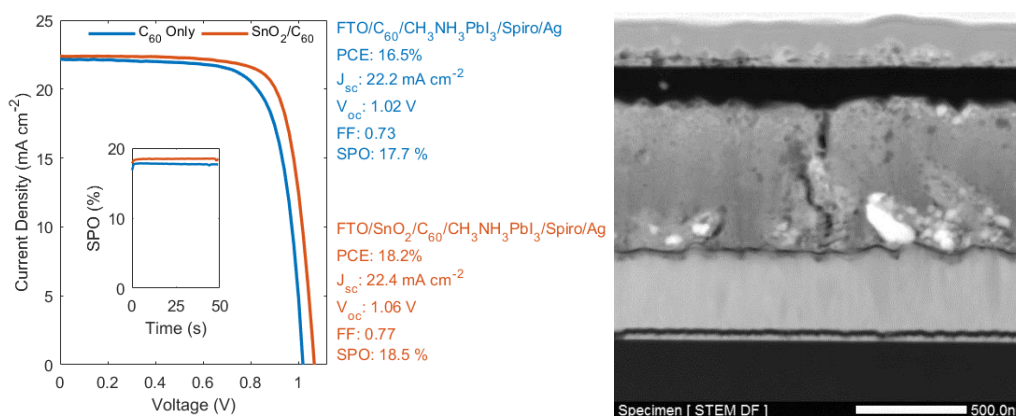


Figure S10 a) Current-voltage curves of the champion devices from the same batch of different device architectures. b) A STEM cross sectional image of a device with a thin layer of SnO_2 and C_{60} .

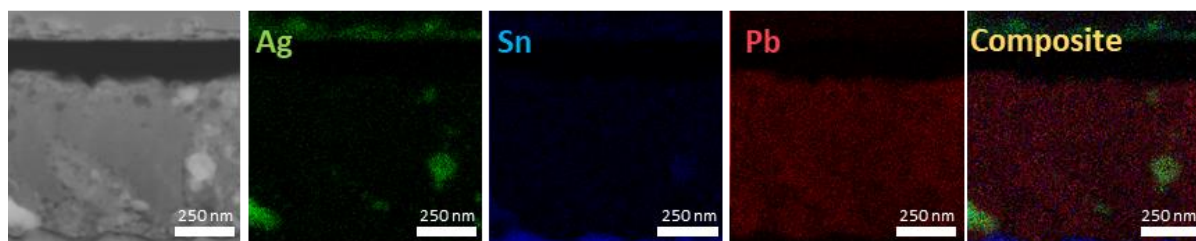


Figure S11. a) HAADF image of a cross-section of a perovskite device and corresponding false color EDS maps of b) Ag c) Sn d) Pb e) overlay of all the maps, to show the elemental composition of the cross-section. The maps show that there is diffusion of Ag through the device.

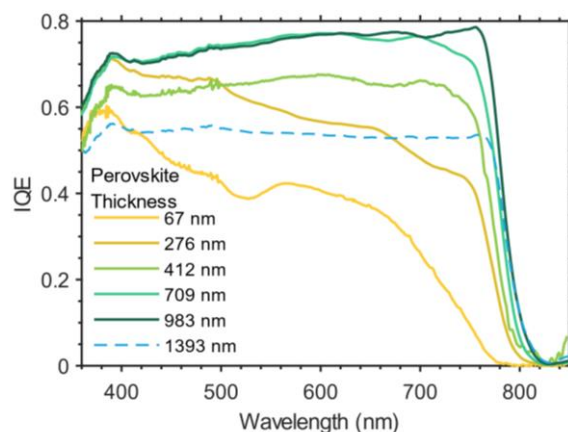


Figure S12 the measured internal quantum efficiency of the devices. The IQE was calculated using the measured absorbance spectra of the device and the external quantum efficiency (EQE) of the device ($\text{IQE} = \text{EQE} / \text{Absorbance}$). The IQE shows the probability of charge carriers being extracted per absorbed photon.

The optical interference observed in the EQE spectra for the devices are due to the reflection losses in the absorption spectra, when these losses are considered it can be observed in the IQE that the devices are converting the absorbed photons efficiently. The change in the absorption, EQE and IQE spectra as the thickness of the perovskite is changed, exemplifies the importance of considering the implications of poor light management in a device.

Optical Simulations

The optical simulations were carried out using a transfer matrix created by Burkhard et al, and can be found from the following [publication](#).^[10] In brief the model builds upon calculations based from the works of Peumans et al and Pettersson et al.^[11,12] To model the optical field, the model treats the light transmitted through the thick glass layer (2 mm) as incoherent which is calculated using Fresnel equations. Thereafter a transfer matrix formalism is used by inputting the refractive indices of each layer in the device stack to account for the absorption of each layer. Values for the complex refractive index of C₆₀, thermally evaporated CH₃NH₃PbI₃, Spiro-OMeTAD were obtained by fitting reflection and transmission data against a transfer matrix model, which is described previously in Crothers *et al.*^[3] The

thickness of each layer was established by globally fitting the layer thickness across all wavelengths, while at each wavelength, the real and complex part of the refractive index were fitted against the reflection and transmission data for each layer on quartz or $\text{CH}_3\text{NH}_3\text{PbI}_3$:quartz. The complex refractive index of SnO_2 , SiO_2 , FTO and Au were used from the study by Ball et al.^[6] The results of the optical simulation shows the wavelength dependent optical electric field within the device and the absorption of each layer.

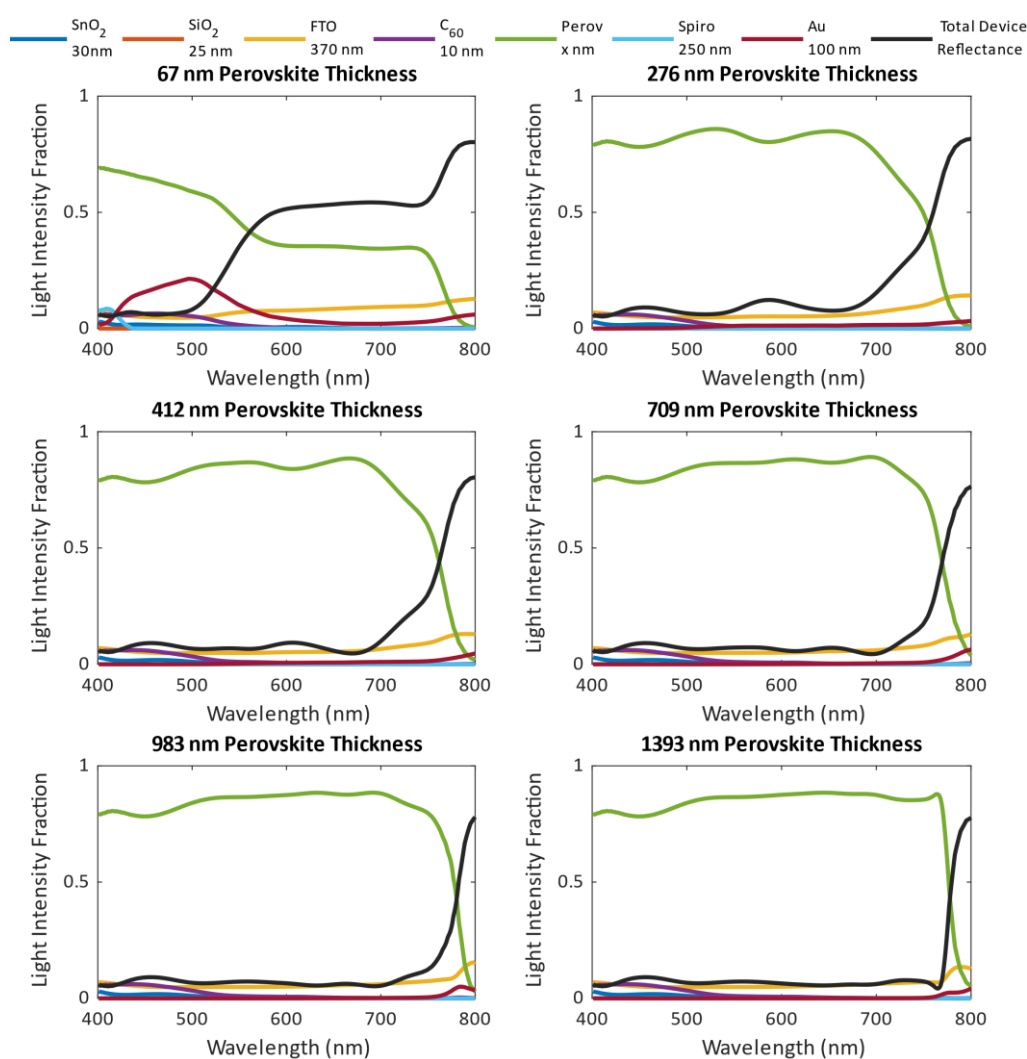


Figure S13. Optical simulations of the fraction of light absorbed. The simulated spectra show the light absorption of the different layers of the devices with the thicknesses shown in the legend, and the perovskite thin film thickness on top of the graphs. The black line shows the total device reflectance. The total device reflectance was used to calculate the device absorptance in Figure 2 (Absorption=1-Reflection)

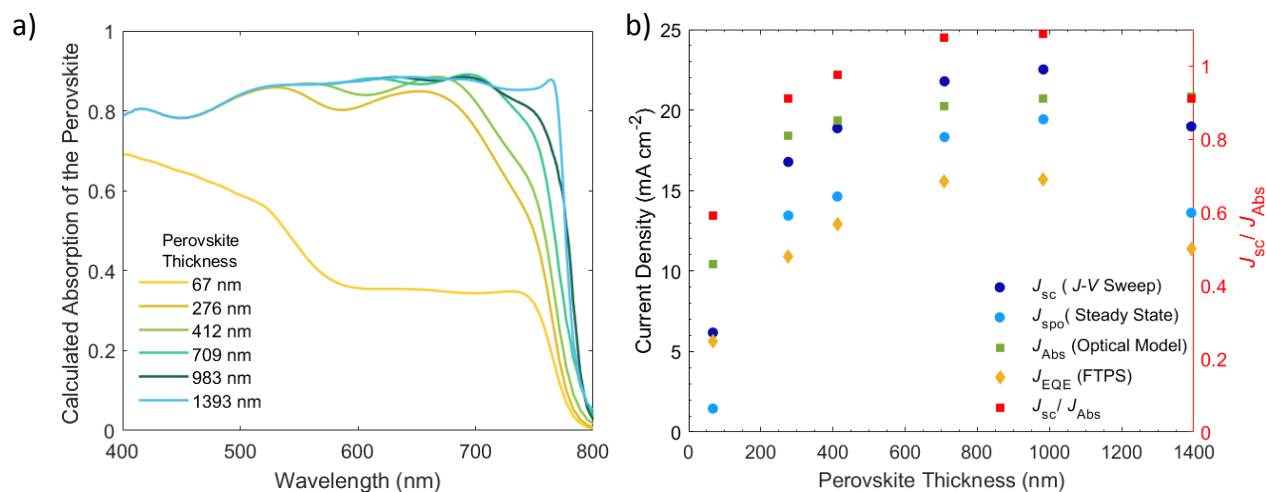


Figure S14 a) The calculated absorption of the perovskite films in the devices shown in Figure 1. Spectra are limited to the range of available dielectric function data, (i.e. 401 nm - 800 nm) **b)** The current density, J , of the devices shown in Figure 1 extracted using different methods. The J_{sc} was extracted from the current voltage sweep under AM 1.5, 1 sun conditions, with 5 seconds prebiasing. The J_{spo} was extracted when the devices were kept at a steady state bias (~voltage at max power point) for period of time as describe in experimental details. The J_{Abs} was calculated by integrating the product of the calculated absorption of the perovskite film and photon flux of the solar spectrum (ASTM-G173-Global Tilt) over the range of the calculate absorption range (401 nm - 800 nm). As current generated for wavelength less than 401nm is not included in this calculation, the value of J_{Abs} will be an underestimate. The J_{EQE} is the integrated current density of the EQE spectra in Figure 2b. The ratio between the J_{sc} and J_{Abs} gives an approximate indication of the charge extraction efficiency in the devices incorporating different perovskite film thicknesses. The values of J_{sc}/J_{Abs} are a slight over estimation owing to the underestimate of J_{Abs} mentioned above.

Figure S14, shows that the current density, J , has a large variation depending on how it was measured and the electrical and environmental conditions it was measured in. The integrated J_{EQE} is much lower than the J_{sc} , as there is no light soaking or prebiasing. However, the general trend of the measured J is the same, there is an increase in J as the perovskite film thickness is increased to ~709 nm and then there is a decrease after the perovskite thickness

increases from ~983 nm. From the calculated absorption spectra, the J plateaus after ~709 nm, however the measured values of J all decrease, highlighting the loss in charge extraction efficiency, as the perovskite film becomes too thick and there is the rise of a perovskite dead volume.

References

- [1] E. H. Anaraki, A. Kermanpur, L. Steier, K. Domanski, T. Matsui, W. Tress, M. Saliba, A. Abate, M. Grätzel, A. Hagfeldt, J.-P. Correa-Baena, *Energy Environ. Sci.* **2016**, *9*, 3128.
- [2] J. Borchert, R. L. Milot, J. B. Patel, C. L. Davies, A. D. Wright, L. Martínez Maestro, H. J. Snaith, L. M. Herz, M. B. Johnston, *ACS Energy Lett.* **2017**, *2*, 2799.
- [3] T. W. Crothers, R. L. Milot, J. B. Patel, E. S. Parrott, J. Schlipf, P. Müller-Buschbaum, M. B. Johnston, L. M. Herz, *Nano Lett.* **2017**, *17*, 5782.
- [4] C. L. Davies, J. B. Patel, C. Q. Xia, L. M. Herz, M. B. Johnston, *J. Infrared, Millimeter, Terahertz Waves* **2018**, *39*, 1236.
- [5] T. Seifert, S. Jaiswal, M. Sajadi, G. Jakob, S. Winnerl, M. Wolf, M. Kläui, T. Kampfrath, *Appl. Phys. Lett.* **2017**, *110*, 252402.
- [6] J. M. Ball, S. D. Stranks, M. T. Hörantner, S. Hüttner, W. Zhang, E. J. W. Crossland, I. Ramirez, M. Riede, M. B. Johnston, R. H. Friend, H. J. Snaith, *Energy Environ. Sci.* **2015**, *8*, 602.
- [7] N. K. Noel, S. N. Habisreutinger, B. Wenger, M. T. Klug, M. T. Hörantner, M. B. Johnston, R. J. Nicholas, D. T. Moore, H. J. Snaith, *Energy Environ. Sci.* **2017**, *10*, 145.
- [8] J. Bisquert, L. Bertoluzzi, I. Mora-Sero, G. Garcia-Belmonte, *J. Phys. Chem. C* **2014**, *118*, 18983.
- [9] I. Mora-Seró, G. Garcia-Belmonte, P. P. Boix, M. A. Vázquez, J. Bisquert, *Energy Environ. Sci.* **2009**, *2*, 678.
- [10] G. F. Burkhard, E. T. Hoke, M. D. McGehee, *Adv. Mater.* **2010**, *22*, 3293.
- [11] P. Peumans, A. Yakimov, S. R. Forrest, *J. Appl. Phys.* **2003**, *93*, 3693.
- [12] L. A. A. Pettersson, L. S. Roman, O. Inganäs, *J. Appl. Phys.* **1999**, *86*, 487.